## REFERENCES

[1] C. A. Burrus and R. W. Dawson, "Small-area high-current-density GaAs electroluminescent diodes and a method of operation for improved degradation characteristics," *Appl. Phys. Lett.*, vol. 17, pp. 97–99, 1970.

[2] C. A. Burrus and E. A. Ulmer, Jr., "Efficient small-area GaAs–$Ga_{1-z}Al_zAs$ heterostructure electroluminescent diodes coupled to optical fibers," *Proc. IEEE*, vol. 59, pp. 1263–1264, Aug. 1971.

[3] C. A. Burrus and B. I. Miller, "Small-area, double-heterostructure aluminum-gallium arsenide electroluminescent diode sources for optical-fiber transmission lines," *Opt. Commun.*, to be published.

[4] J. J. Brophy, "Fluctuations in luminescent junctions," *J. Appl. Phys.*, vol. 38, pp. 2465–2469, 1967.

[5] G. Guekos and M. J. O. Strutt, "Current noise spectra of GaAs laser diodes in the luminescence mode," *IEEE J. Quantum Electron.* (Corresp.), vol. QE-4, pp. 502-503, Aug. 1968.

[6] G. Guekos and M. J. O. Strutt, "Correlation between laser emission noise and voltage noise in GaAs CW laser diodes," *IEEE J. Quantum Electron.* (Corresp.), vol. QE-5, pp. 129–130, Feb. 1969.


# Astigmatically Compensated Cavities for CW Dye Lasers

HERWIG W. KOGELNIK, MEMBER, IEEE,
ERICH P. IPPEN, MEMBER, IEEE, ANDREW DIENES, AND CHARLES V. SHANK

***Abstract*—An analysis is given of folded 3-mirror laser resonators with an internal cell set at Brewster's angle. A method is described to compensate the astigmatic distortions introduced by both the internal mirror and the cell. This compensation is achieved for a specific relation between cell thickness and folding angle. It allows the formation of a tight intracavity focus as required in applications such as CW dye lasers. A discussion is given of the mode characteristics of compensated cavities and of the limitation on beam concentration set by the thickness of the Brewster cell.**

## I. INTRODUCTION

IN CW dye-laser applications [1]–[3] there is a need for cavity designs that provide an intracavity focus where the modal beam is highly concentrated (to typical beam diameters of 10 $\mu$m). This small spot is demanded by pumping requirements. In addition, it is desirable to have fairly long cavity length (of typically 1 m) for tuning and mode-locking purposes. Cavities of this kind have other applications. One example is a cavity-dumping system [4] where an acoustooptic deflector is positioned at the focus to allow high-speed operation. Another application is in the passive mode locking of low-gain lasers [5].

Cavity configurations that satisfy the seemingly contradictory requirements of long length and tight focus are resonators with internal lenses [1]. An equivalent system is a three-mirror resonator such as shown in Fig. 1. This is often preferred [2]–[5] because the reflection losses of the center mirror can in practice be kept to much smaller values than the Fresnel and bulk losses of the internal lens. Such a folded cavity, however, requires an oblique angle of incidence at the center mirror and introduces astigmatic distortions that limit the performance of the system. In addition, the above group of applications requires an optical element to be inserted at the focus (i.e., the dye cell or the acoustooptic plate). This element is preferably inserted at the Brewster angle to minimize Fresnel losses. A Brewster window also has astigmatic properties that can limit the performance of the system. The effect of either astigmatic distortion becomes more severe the smaller the desired spot size. We have found it possible to design a three-mirror laser resonator with an internal Brewster-angle cell that is astigmatically compensated. The compensation is achieved by offsetting the distortions of the center mirror by those of the Brewster cell. If, on the other hand, a Brewster-angle cell is used in an "in line" resonator with an internal lens [1], then only the astigmatism of the cell is present and no compensation is possible.

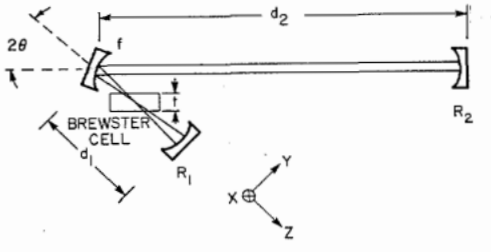


Fig. 1. Folded 3-mirror cavity with internal Brewster-angle cell.

Manuscript received October 27, 1971.
The authors are with Bell Telephone Laboratories, Inc., Holmdel, N. J. 07733.

In the following, we will first discuss the properties of small-spot cavities, then we will describe the astigmatic properties of mirrors and Brewster-angle cells and how they can be used to compensate each other. This paper is concluded by a discussion of the properties of compensated small-spot resonator systems.

## II. Small-Spot Cavity With Internal Lens

To prepare the ground for the discussion of compensated cavities we will recapitulate, in this section, the properties of resonators with an internal lens. The properties of interest are the resonator stability, the location of the beam focus or "beam waist", and the beam radius at the waist. Expressions for these quantities are available in the literature [6], but we will cast these into a form that is geared towards the achievement of a tight internal focus and that makes transparent the behavior of the system.

Fig. 2 shows a resonator with an internal lens of focal length $f$. The spacings between the lens and the mirrors are $d_1$ and $d_2$ and the curvature radii of the mirrors are $R_1$ and $R_2$. To achieve a small internal spot or focus, one designs the system with a large spacing $d_2 \gg f$ and a short spacing $d_1$ that is approximately $d_1 \approx R_1 + f$. The small spot is produced in the vicinity of the center of curvature of the mirror $R_1$, i.e., in the short leg of the system.

To analyze this system we can use the imaging rules of [7]. These allow us to replace the combination of mirror $R_2$ and the lens by a single equivalent mirror $R'_2$, which is indicated in Fig. 2. The result is an equivalent resonator that is empty and to which we can apply standard formulas. The imaging rules give us the mirror spacing as

$$d = d_1 - d_2 f/(d_2 - f), \tag{1}$$

and the curvature radius $R'_2$

$$R'_2 = R_2 f^2/(d_2 - f)(d_2 - R_2 - f). \tag{2}$$

In small-spot systems of this type, the adjustment of the spacing $d_1$ is critical, as the cavity is stable only over a small range of values (typically a few millimeters) near $d_1 = R_1 + f$. It is, therefore, convenient to define an adjustment measure $\delta$ by

$$d_1 \equiv R_1 + f + \delta. \tag{3}$$

The *stability range* of the resonator extends from a adjustment value $\delta_{\min}$ to a maximum value $\delta_{\max}$, which we can calculate from the usual stability conditions [6] (i.e., $d = R_1 + R'_2$ and $d = R_1$). We obtain

$$\delta_{\min} = f^2/(d_2 - R_2 - f)$$
$$\delta_{\max} = f^2/(d_2 - f). \tag{4}$$

For the stability range $2S$ we get

$$2S \equiv \delta_{\max} - \delta_{\min} = -R_2 f^2/(d_2 - f)(d_2 - R_2 - f). \tag{5}$$

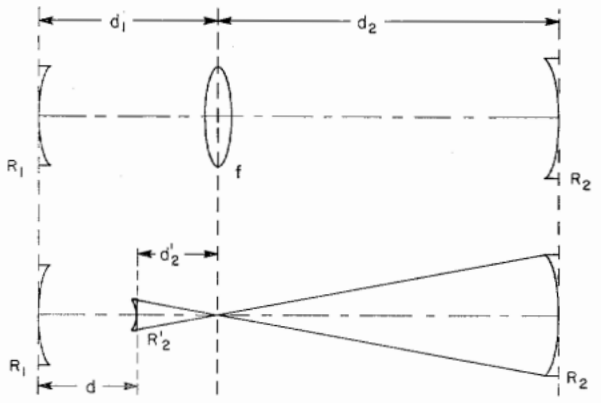


Fig. 2. Resonator with internal lens and equivalent empty resonator.

In small-spot designs we usually have $d_2 \gg f$ and $R_2 \approx \infty$, which leads to stability ranges that are approximately $2S \approx f^2/d_2$.

The next quantity of interest is the *location of the beam waist* where the mode of the resonator is focused to a small spot. For the distance $t_1$, from mirror $R_1$ to the waist, we have the expression [6]

$$t_1 = d(R'_2 - d)/(R_1 + R'_2 - 2d). \tag{6}$$

After inserting (1)–(5) we can rewrite this in the form

$$t_1 = (R_1 + \delta - \delta_{\max}) \cdot (R_1 + \delta - \delta_{\min})/(R_1 + 2\delta - \delta_{\max} - \delta_{\min}). \tag{7}$$

In inspecting this formula, it should be noted that the waist location $t_1$ stays very much fixed at $R_1$ as one adjusts the mirror-lens spacing $d_1$ through the stability range. We have

$$t_{1\,\max} = t_{1\,\min} = R_1$$
$$t_{1\,\text{center}} = R_1 - S^2/R_1. \tag{8}$$

At the limits of the range, the waist location is exactly $R_1$ and at the center of the range (i.e. for $2\delta = \delta_{\max} + \delta_{\min}$), $t_{1\,\text{center}}$ deviates only a little from $R_1$. As a numerical illustration, consider the parameters of a system used in dye-laser experiments [2], where $R_1 = f = 5$ cm, $d_2 = 190$ cm, and $R_2 = \infty$. This resonator has a stability range of $2S = 1.3$ mm. In the range center the waist location deviates from $R_1$ by $S^2/R_1 = 8.5$ $\mu$m, indeed, a small deviation.

The third quantity of interest is the *beam diameter at the waist*. The waist radius $w_0$ is given by the formula [6]

$$(\pi w_0^2/\lambda)^2 = d(R_1 - d)(R'_2 - d) \cdot (R_1 + R_2 - d)/(R_1 + R_2 - 2d)^2. \tag{9}$$

After inserting (1)–(5), we get, after some algebra,

$$(\pi w_0^2/\lambda)^2 = \frac{(R_1+\delta-\delta_{\max})(R_1+\delta-\delta_{\min})(\delta_{\max}-\delta)(\delta-\delta_{\min})}{(R_1+2\delta-\delta_{\max}-\delta_{\min})^2}$$
$$\approx (\delta_{\max} - \delta)(\delta - \delta_{\min}). \tag{10}$$

Here the approximate expression is good as long as $R_1$ is large compared to the stability range $2S$. We see that $w_0 = 0$ at the limits of the stability range. As $d_1$ is tuned away from these limits, $w_0$ increases rapidly reaching a rather flat plateau that extends almost throughout the range (see Fig. 4). In the range center we have

$$(\pi w_0^2/\lambda)_{\text{center}}^2 = S^2(1 - S^2/R_1^2). \tag{11}$$

For $R_1 \gg S$ the second term is negligibly small and we can write for the confocal parameter $b$ of the mode

$$b = 2\pi w_0^2/\lambda \approx 2S \approx f^2/d_2. \tag{12}$$

This implies that for a small-spot cavity, which is adpusted near the center of its stability range, the *confocal parameter of the modal beam is equal to the stability range.*

Related to the confocal parameter is the far-field angle $\phi$ of the beam, which is

$$\phi = \lambda/\pi w_0 \approx \sqrt{\lambda/\pi S}. \tag{13}$$

From this follows the beam radius at the lens

$$w_{\text{lens}} \approx f \cdot \phi \approx f\sqrt{\lambda/\pi S} \approx \sqrt{\lambda d_2/\pi}. \tag{14}$$

## III. Astigmatic Elements

In a three-mirror cavity of the type shown in Fig. 1, there are two optical elements that introduce astigmatic distortions, the center mirror and the Brewster-angle cell. This astigmatism means that geometrical ray bundles in the (sagittal) $xz$ plane behave differently than ray bundles in the (tangential) $yz$ plane. In this section we will characterize the two optical elements within the paraxial ray formalism. This will give us the elements of the corresponding ray matrices, which can then be used to determine the properties of the resonator modes in the Gaussian-beam approximation [6] ($ABCD$-law).

### *A) Mirror Astigmatism*

It is well known [8] that a mirror used at oblique incidence focuses sagittal ($xz$) ray bundles at a different location than tangential ($yz$) bundles. This is reflected in two different effective focal lengths $f_x$ and $f_y$, which are related to the actual focal length $f$ of the mirror by

$$f_x = f/\cos\theta$$
$$f_y = f \cdot \cos\theta, \tag{15}$$

where $\theta$ is the angle of incidence as shown in Fig. 1.

### *B) Brewster-Cell Astigmatism*

A Brewster cell or Brewster-angle window also acts differently on the sagittal and the tangential ray bundles. This action can be expressed by two different effective distances $d_x$ and $d_y$, which the rays have to traverse [9]. A precise definition of the concept of an effective distance is provided by the ray-matrix formalism. The distances $d_x$ and $d_y$ can be derived from Snell's law and also by using Huygen's principle [9]. Yet another derivation

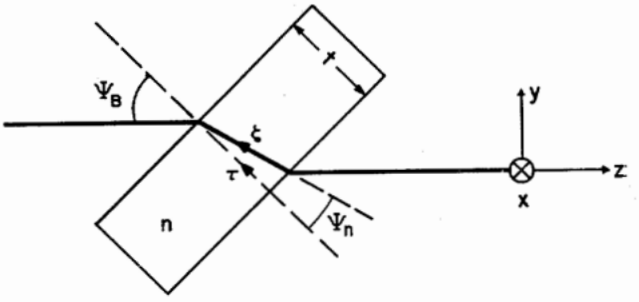


Fig. 3. Brewster-angle cell geometry. Coordinates and parameters used in analysis are shown.

using the propagation laws for Gaussian beams is indicated in Section V. Referring to the geometry shown in Fig. 3 and a Brewster window of thickness $t$ and refractive index $n$, one gets

$$d_x = t\sqrt{n^2 + 1}/n^2$$
$$d_y = t\sqrt{n^2 + 1}/n^4. \tag{16}$$

## IV. Compensation of Three-Mirror Cavities

We consider, now, resonator systems of the type shown in Fig. 1, which have two internal astigmatic elements, the center mirror, and the Brewster cell. To analyze such systems, the assumptions and the results of Section II can be used. However, the astigmatism makes it necessary to consider the ray and mode characteristics of the sagittal ($xz$) and the tangential ($yz$) planes separately. To make this distinction, we will use the subscripts $x$ and $y$. Following Section II, two adjustment measures $\delta_x$ and $\delta_y$ are defined by

$$d_{1x} \equiv R_1 + f_x + \delta_x = d_{\text{air}} + d_x$$
$$d_{1y} \equiv R_1 + f_y + \delta_y = d_{\text{air}} + d_y \tag{17}$$

where $f_x$ and $f_y$ are the effective focal lengths of the center mirror, and $d_x$ and $d_y$ are the effective distances of the Brewster cell, as discussed in the previous section. The effective mirror-lens separation $d_{1x}$ and $d_{1y}$ are made up of the respective cell distances $d_x$ and $d_y$ and of the optical-path distance in air $d_{\text{air}}$, which is the same for the $x$ and the $y$ cases.

Let us, first, inspect the stability limits $\delta_{\max}$ and $\delta_{\min}$ and the stability range $2S$. In the presence of astigmatism, these quantities are, in principle, different for $x$ and $y$. Equations (4) and (5) show that the dominant factor causing a change in these quantities is the astigmatism of the center mirror. The factor $f^2$ appearing in these equations has to be modified to $f_x^2$ and $f_y^2$. However, in practice, these factors do not differ very much, as the practical angles of incidence $\theta$ are very small. For $\theta = 6°$, for example, we have $\cos^2 6° = 0.99$, which implies that the mirror astigmatism leads to a one-percent increase in the sagittal stability range and limits and to a corresponding decrease in the tangential quantities. The quantities $\delta_{\max}$, $\delta_{\min}$, and $2S$ are, therefore, essentially the same for $x$ and $y$, which allows a considerable sim-

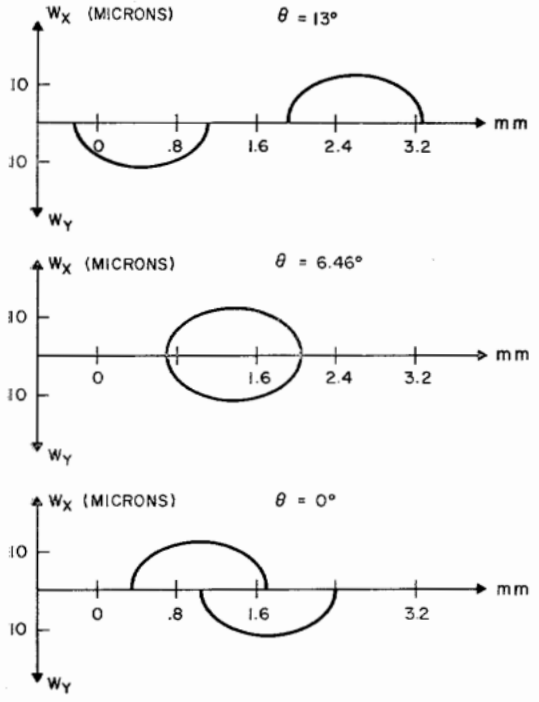


Fig. 4. Beam waist radii and stability ranges for a folded 3-mirror cavity for various angles of incidence $\theta$ at center mirror. The horizontal scale measures the relative adjustment of $d_1$ $f_{\bar{x}}$ and $w_Y$ are the beam waist radii in the $xz$ and $yz$ planes, respectively. The cavity parameters are $R_1 = 5$ cm, $R_2 = \infty$, $f = 5$ cm, $d_2 = 190$ cm, $d_1 \approx 10$ cm, $t = 1.5$ mm, $n = 1.45$, and $\lambda = 0.57$ $\mu$m.

plification of our argument. It is important to note, however, that the $x$ and $y$ values of these limits occur at *different* values of $d_{\text{air}}$.

The adjustment measures $\delta_x$ and $\delta_y$ are, in general, different. These measures depend on the adjustment of $d_{\text{air}}$, as indicated by (17). For a given $d_{\text{air}}$, the resonator will generally operate in a different portion of the $x$ stability range than that of the $y$ stability range. In fact, it is possible that a resonator is stable in $x$ and unstable in $y$, as illustrated in Fig. 4.

The purpose of an astigmatic compensation is to produce a maximum overlap of the $x$- and $y$-stability ranges, which should lead to adjustment measures and mode characteristics that are more or less equal in $x$ and $y$ (we shall see later that some differences remain even after compensation). We can calculate the difference in the adjustment measures from (17) and obtain

$$\delta_x - \delta_y = (d_x - d_y) - (f_x - f_y)$$
$$= t(n^2 - 1)\sqrt{n^2 + 1}/n^4 - f \sin\theta \tan\theta. \quad (18)$$

When the adjustment measures are equal, the resonator operates in corresponding portions of the $x$ and $y$ stability ranges and we have compensation. According to (18), this is assured when

$$2Nt = 2f \sin\theta \tan\theta \equiv R \sin\theta \tan\theta \quad (19)$$

where

$$N = (n^2 - 1)\sqrt{n^2 + 1}/n^4. \quad (20)$$

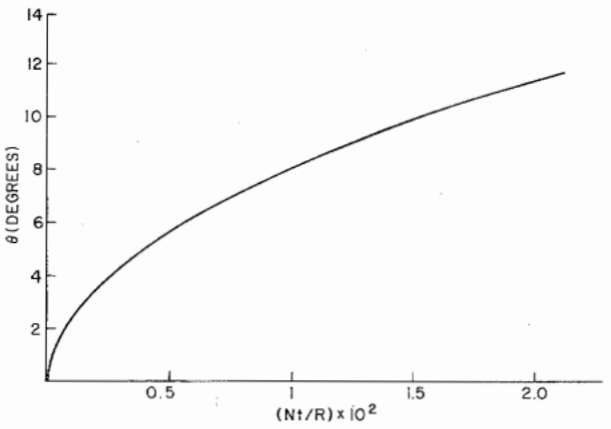


Fig. 5. Compensation angle versus normalized cavity parameter $Nt/R$.

This shows that we can achieve compensation by trading the cell thickness $t$ for the angle of incidence $\theta$ on the center mirror. Fig. 5 shows a normalized plot of the relation between $t$ and $\theta$ leading to compensation (19). The factor $N$ is a function of the refractive index $n$ only. A selection of numerical values for $N$ is given in the following table.

| $n$ | 1.3 | 1.4 | 1.5 | 1.6 | 1.7 |
|---|---|---|---|---|---|
| $N$ | 0.396 | 0.430 | 0.445 | 0.449 | 0.446 |

It should be noted that the above compensation can only be achieved for the cell orientation shown in Fig. 1, i.e., for a common plane of incidence, for both center mirror and Brewster cell. If the two planes of incidence are oriented perpendicular to each other, then the astigmatic effects add and compensation is impossible.

## V. Properties of Compensated Cavities

In this section we will investigate in further detail the properties of compensated three-mirror cavities and, in particular, the characteristics of the modal beam inside and outside the Brewster cell.

Fig. 4 illustrates the effects of compensation for our numerical example from above, using values $n = 1.45$, $t = 1.5$ mm, and $\lambda = 0.57$ $\mu$m. In this figure we plot the sagittal ($w_x$) and the tangential ($w_y$) beam-waist radii as a function of the relative adjustment of the distance $d_1$. From (10) $w_x$ and $w_y$ are calculated and the region for which one gets real $w$ values indicates the stability range. We note that for $\theta = 0$ only one half of the $x$-stability range overlaps the $y$ range. For $\theta = 6.46°$ compensation and good overlap of the stability ranges are achieved. In the center of the common range, the waist radii $w_x$ and $w_y$ are approximately the same and they are relatively stationary with respect to a change in $d_1$. For $\theta = 13°$ there is no stability overlap at all, and the cavity is always unstable in at least one of the $x$ or $y$ coordinates.

The approximate equality of $w_x$ and $w_y$ holds quite generally, not just for the above numerical example.

It follows from the equality of the stability ranges ($2S_x \approx 2S_y$), which we have demonstrated previously. Inserting this into (11), we get for the waist radii in the center of the stability range

$$w_x \approx w_y = w_0. \tag{21}$$

In addition, it follows from (8) that the effective distances $t_{1x}$ and $t_{1y}$ from the mirror $R_1$ to the $x$ and $y$ waists are approximately equal

$$t_{1x} \approx t_{1y} \approx R_1. \tag{22}$$

The above relations are very simple and they specify the beam in the short leg of the cavity. It must be kept in mind, however, that the above parameters refer to the properties of the beam *in air*. For dye-laser applications, we also need to know the behavior of the beam *inside the Brewster cell*, which contains the dye and where a high intensity is required. The remainder of this section is devoted to the investigation of this behavior. In particular, we shall derive the obtainable beam concentration in the cell.

First we recall (16), which tells us that the effective distances in the Brewster cell are measured differently in $x$ and $y$. Then we choose position of the cell, which is such that the beam waists occur inside the cell. The effective mirror-to-waist spacings are now made up of two parts, the distance $t_{\text{air}}$ from the mirror to the cell entrance, and the effective distance inside the cell from the entrance to the waists

$$\begin{aligned} t_{1x} &= t_{\text{air}} + \tau_x\sqrt{n^2+1}/n^2 \approx R_1 \\ t_{1y} &= t_{\text{air}} + \tau_y\sqrt{n^2+1}/n^4 \approx R_1. \end{aligned} \tag{23}$$

$\tau_x$ and $\tau_y$ indicate the location of the two waists in the cell measured perpendicular to the cell surface as shown in Fig. 3. These waist locations change as a function of $t_{\text{air}}$. However, it follows from (23), that there is a relation

$$\tau_y \approx n^2\tau_x \tag{24}$$

that is independent of the cell adjustment $t_{\text{air}}$.

We now postulate a *symmetrical* configuration such that the $x$ and $y$ waists are equidistant from the center of the cell. This implies

$$\tau_y + \tau_y = t. \tag{25}$$

This case of symmetry should be very close to a practical optimum. Combining (24) and (25) we get

$$\begin{aligned} \tau_x &= t/(n^2+1), \\ \tau_y &= tn^2/(n^2+1), \\ \Delta\tau &= \tau_y - \tau_x = t(n^2-1)/(n^2+1), \end{aligned} \tag{26}$$

where $\Delta\tau$ is the spacing between the $x$ and $y$ waists in the cell. For our numerical example of $n = 1.45$, we find that $\tau_x \approx t/3$, $\tau_y \approx 2t/3$, and $\Delta\tau \approx t/3$, i.e., waists that are spaced by about one third of the cell thickness.

Next we have to consider the change in beam radius $w_y$, which takes place when a beam enters a Brewster cell. This change is the consequence of the refractional change of the direction of propagation and it can be calculated from a simple geometrical projection. For a beam with radius $w$ just before entering the cell, we get the in-cell beam radii

$$\begin{aligned} w_x &= w \\ w_y &= w\cdot\cos\Psi_n/\cos\Psi_B = nw, \end{aligned} \tag{27}$$

where $\Psi_B$ is the angle of incidence in air (Brewster's angle), which obeys $\tan\Psi_B = n$, and $\Psi_n$ is the corresponding angle in the cell medium.

As shown in Fig. 3 we use the parameter $\zeta$ to measure the propagation distance along the beam axis inside the cell. It is related to the cell-depth parameter (measured perpendicular to the cell surface) by

$$\zeta = \tau/\cos\Psi_n = \tau\sqrt{n^2+1}/n. \tag{28}$$

Now we apply the laws of beam expansion by diffraction [6]. In air the beam radius $w$ ($z$) expands as

$$w(z) = w_0\sqrt{1 + (\lambda z/\pi w_0^2)^2}, \tag{29}$$

where $z$ is measured from the beam waist and $w_0$ is the waist radius. Assuming for the moment that the beam waist is located at the cell entrance, we apply (27) and obtain for the expansion of beam radii inside the cell

$$\begin{aligned} w_x(\zeta) &= w_0\sqrt{1 + (\lambda\zeta/\pi n w_0^2)^2} \\ w_y(\zeta) &= nw_0\sqrt{1 + (\lambda\zeta/\pi n^3 w_0^2)^2}, \end{aligned} \tag{30}$$

where the reduced wavelength ($\lambda/n$) in the cell medium has been taken into account.

The reader will take note that at this point we have an alternate devrivation of (16). Comparing (29) and (30) effective path lengths can be assigned to the cell. In this comparison, we have to use (28) and the result agrees with the effective cell distances given in (16). The difference between $d_x$ and $d_y$ is seen to be a direct consequence of the geometrical change of $w_y$ on entry into the cell.

In order to be able to determine the beam intensity in the Brewster cell, it is necessary to know the cross-sectional beam area $A$ ($\zeta$) $\equiv \pi w_x w_y$. To allow for different waist locations $\zeta_x$ and $\zeta_y$, we write

$$\begin{aligned} A(\zeta) &= \pi w_x w_y \\ &= \pi n w_0^2\sqrt{1 + (\lambda/\pi n w_0^2)^2(\zeta-\zeta_x)^2} \\ &\quad\cdot\sqrt{1 + (\lambda/\pi n^3 w_0^2)^2(\zeta-\zeta_y)^2} \end{aligned} \tag{31}$$

where we have used (30). For the special case of symmetrically arranged waist locations we have found with (26) and (28)

$$\begin{aligned} \zeta_x &= t/n\sqrt{n^2+1} \\ \zeta_y &= tn/\sqrt{n^2+1}. \end{aligned} \tag{32}$$

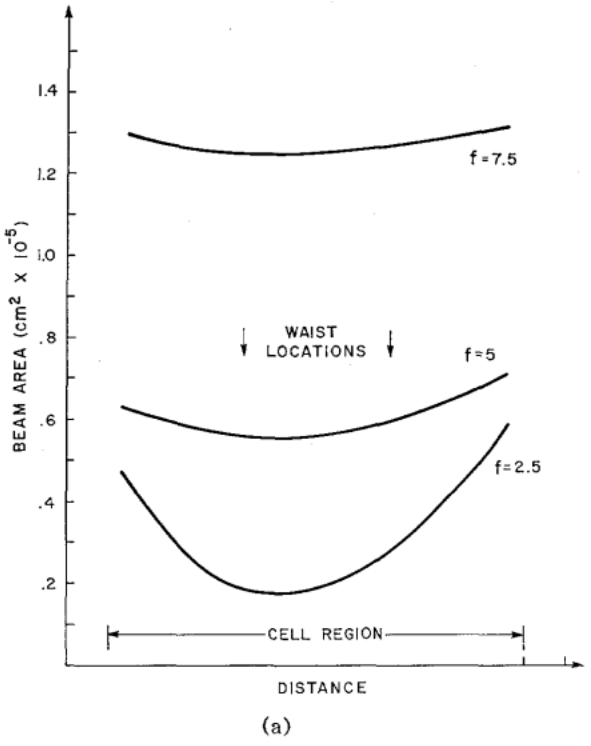


(a)

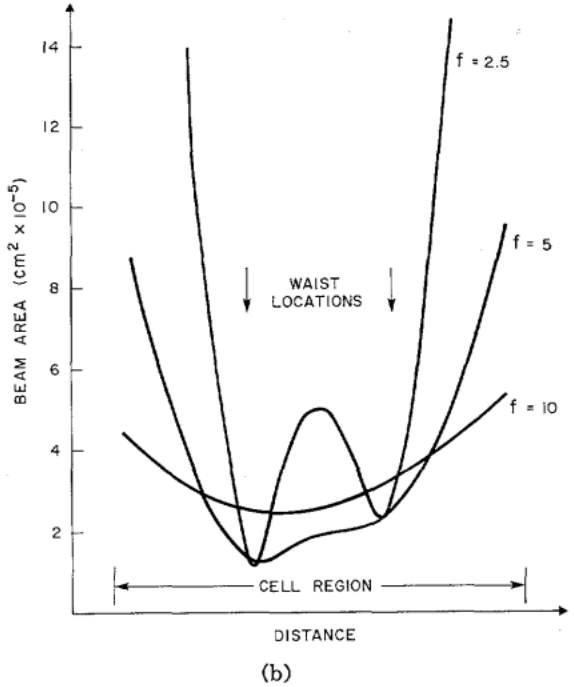


(b)

Fig. 6. Beam area versus distance ($\zeta$) in the Brewster cell for a compensated cavity with various focal lengths of the center mirror. (a) $t = 1$ mm. (b) $t = 10$ mm. Other cavity parameters are same as in Fig. 4.

Fig. 6 illustrates the variation of the beam area $A$ as a function of the distance $\zeta$ in the cell for the symmetrical case and for two different cell thicknesses $t$. The cavity parameters are those used in our previous numerical examples with several values for the focal length $f$ of the center mirror. Fig. 6(a) shows the situation for a 1-mm-thick cell. The waist locations $\zeta_x$ and $\zeta_y$ are marked on the plot. We note that $A$ varies approximately as a

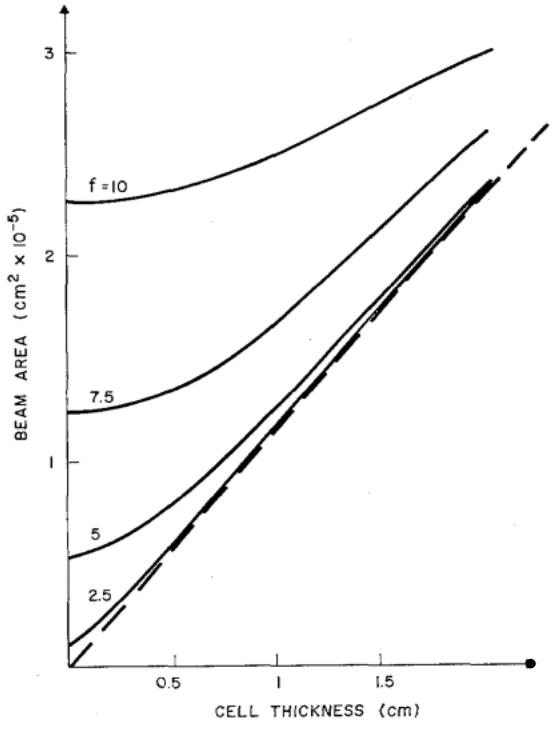


Fig. 7. Minimum beam area versus cell thickness for various focal lengths of the center mirror. Other cavity parameters are same as in Fig. 4.

hyperbola. For large values of $f$ the beam focus (minimum $A$) occurs approximately in cell center, shifting somewhat towards $\zeta_x$ (the small waist radius) for decreasing values of $f$.

Fig. 6(b) shows a similar plot for a cell thickness of $t = 1$ cm. There we notice the limiting effect of the cell thickness on the achievable beam concentration. As before, the beam concentration tends to improve as $f$ is decreased. But at values lower than $f \approx 5$ cm, a double minimum develops and the beam area in the cell center increases again. The minima occur near the waist locations $\zeta_x$ and $\zeta_y$ where the beam areas seem to have become insensitive to changes in $f$. For this case, $f = 5$ cm is a better choice than $f = 2.5$ cm and we do not gain in beam concentration by reducing $f$ beyond that value.

Inspecting (31), the two extremes for the behavior illustrated above are found to depend on the relative magnitudes of the confocal beam parameter (i.e., the stability ranges) and the cell thickness $t$. For $S \approx \pi w_0^2/\lambda \gg t$, we obtain for ($\zeta = \zeta_x$)

$$A \approx \pi n w_0^2 \approx n\lambda S \approx n\lambda f^2/d_2, \tag{33}$$

i.e., a beam area that is approximately equal to the product between wavelength and stability range. In the limit of large cell thickness $t \gg S$, we get (also at $\zeta = \zeta_x$)

$$A \approx \lambda t(n^2 - 1)/n^3\sqrt{n^3 + 1}, \tag{34}$$

which tells us that the achievable minimum beam area is now limited by the cell thickness. For $n \approx 1.45$, this limit is approximately $A = 0.2\lambda t$.

Fig. 7 illustrates how the minimum beam area varies

as a function of cell thickness for various values of $f$. The dashed line indicates the large $t$ limit of (34). The (exactly) calculated intersections of the curves with the ordinate are very nearly at the values predicted by (33).

## VI. Conclusions

We have shown that it is possible to design folded three-mirror cavities such that the astigmatic distortions of the center mirror are compensated by the astigmatism of the internal Brewster cell. The compensation leads to beam characteristics that are quite stable relative to small adjustments of the length of the short leg of the cavity and it allows the achievement of small internal beam spots. However, even with compensation, the thickness of the internal cell limits the minimum attainable beam area to about $0.2\lambda t$, which is usually a much more severe restriction than that posed by the $F$ numbers of the cavity mirrors. The results that we have derived are applicable to any tightly focused system that requires the use of either a Brewster-angle element or an off-axis mirror. In particular, the great beam concentration achievable with the compensated three-mirror cavities have made this system of considerable interest for CW dye-laser applications.

## References

[1] M. Hercher and H. A. Pike, "Tunable dye laser configurations," *Opt. Commun.*, vol. 3, pp. 65–67, Mar. 1971.
[2] R. L. Kohn, C. V. Shank, E. P. Ippen, and A. Dienes, "An intracavity pumped CW dye laser," *Opt. Commun.*, vol. 3, pp. 177–178, May 1971; also, A. Dienes, E. P. Ippen, and C. V. Shank, "High-efficiency tunable CW dye laser," *IEEE J. Quantum Electron*, this issue, p. 388.
[3] A. Dienes, E. P. Ippen, and C. V. Shank, "A mode-locked CW dye laser," *Appl. Phys. Lett.*, vol. 19, pp. 258–260, Oct. 1971.
[4] D. Maydan, "Fast modulator for extraction of internal laser power," *J. Appl. Phys.*, vol. 41, pp. 1552–1559, Mar. 1970.
[5] P. K. Runge, "Mode-locking of He–Ne lasers with saturable organic dyes," *Opt. Commun.*, vol. 3, pp. 434–436, Aug. 1971.
[6] H. Kogelnik and T. Li, "Laser beams and resonators," *Appl. Opt.*, vol. 5, pp. 1550–1567, Oct. 1966.
[7] H. Kogelnik, "Imaging of optical modes—resonators with internal lenses," *Bell Syst. Tech. J.*, vol. 44, pp. 455–494, Mar. 1965.
[8] F. A. Jenkins and H. E. White, *Fundamentals of Optics*. New York: McGraw-Hill, 1957, p. 95.
[9] D. C. Hanna, "Astigmatic Gaussian beams produced by axially asymmetric laser cavities," *IEEE J. Quantum Electron.*, vol. QE-5, pp. 483–488, Oct. 1969.

# Correspondence

## Experimental Tests of Proposed Mechanisms for Gradual Degradation of GaAs Double-Heterostructure Injection Lasers

D. H. NEWMAN, S. RITCHIE, AND S. O'HARA

*Abstract*—**Degradation rates of double-heterostructure GaAs lasers have been measured and found to vary superlinearly with the injected current density above threshold. The results are discussed in the context of the Gold–Weisberg phonon-kick and the extended Longini field-inhibited diffusion degradation mechanisms.**

The purpose of this correspondence is to comment on the difficulties of interpreting the experimental results on gradual degradation of GaAs lasers in terms of either the Gold–Weisberg phonon-kick or the extended Longini field-inhibited diffusion mechanisms [1]. Other mechanisms, including the effect of the environment and transport of impurities on or from surfaces, may also explain experimental results. The objective here is to consider specifically the feasibility of the two mechanisms mentioned above and about which extensive discussion has taken place in the literature [1]–[5].

It does not appear to be generally appreciated in the literature on degradation that theories of laser action in perfect homogeneous p-n junction diodes imply that the gain in the active region saturates at the threshold current and remains constant for steady currents above threshold [6], [7]. The round trip gain must in fact be unity regardless of current density above threshold for steady-state conditions to prevail. As the gain is determined by the separation of the quasi-Fermi levels for electrons and holes [8], the latter become fixed relative to the band edges. Thus in a perfect homogeneous p-n diode laser, all the excess current injected above threshold goes into the stimulated emission process. Also the electron and hole densities in the conduction and valence bands respectively remain constant above the threshold. Hence:

1) any electron-hole recombination process (other than stimulated emission) is held at a fixed rate for all injection current densities greater than threshold;
2) the voltage drop at the junction remains constant above the threshold current density; the current can increase because of the shortened lifetime for electron-hole recombination at the junction due to the stimulated emission process.

It follows that if either the Gold–Weisberg phonon-kick mechanism (dependent on the rate of nonradiative recom-

Manuscript received August 20, 1971; revised November 10, 1971. The devices described in this correspondence were supplied by P. R. Selway and A. R. Goodwin of Standard Telecommunication Laboratories, Harlow, England, under a Ministry of Defense (Navy Department) contract.
The authors are with the British Post Office Research Department, Martlesham Heath, Ipswich, Suffolk, England.